ISSN 1063-7761, Journal of Experimental and Theoretical Physics, 2011, Vol. 113, No. 5, pp. 755–761. © Pleiades Publishing, Inc., 2011.
Original Russian Text © S.Ya. Vetrov, A.Yu. Avdeeva, I.V. Timofeev, 2011, published in Zhurnal Eksperimental'noi i Teoreticheskoi Fiziki, 2011, Vol. 140, No. 5, pp. 871–878.

ATOMS, MOLECULES, OPTICS

Spectral Properties of a One-Dimensional Photonic Crystal with a Resonant Defect Nanocomposite Layer

S. Ya. Vetrov[a,*], A. Yu. Avdeeva[a,], and I. V. Timofeev[b]**

[a] *Siberian Federal University, Svobodny pr. 79, Krasnoyarsk, 660074 Russia*

**e-mail: s.vetrov@inbox.ru*

***e-mail: avdeeva-anstasiya@yandex.ru*

[b] *Kirensky Institute of Physics, Siberian Branch, Russian Academy of Sciences, Akademgorodok, Krasnoyarsk, 660036 Russia*

Received March 9, 2011

Abstract—The spectral properties of a one-dimensional photonic crystal with a defect nanocomposite layer that consists of metallic nanoballs distributed in a transparent matrix and is characterized by an effective resonance permittivity are studied. The problem of calculating the transmission, reflection, and absorption spectra of *p*-polarized waves in such structures is solved for oblique incidence of light, and the spectral manifestation of defect-mode splitting as a function of the volume fraction of nanoballs and the structural parameters is studied. The splitting is found to depend substantially on the nanoball concentration in the defect, the defect layer thickness, and the angle of incidence. The angle of incidence is found at which the resonance frequency of the nanocomposite is located near the edge of the bandgap or falls in the frequency region of a continuous spectrum. The resonance situation appearing in this case results in an additional transmission band or an additional bandgap in the transmission spectrum.

DOI: 10.1134/S1063776111140093

1. INTRODUCTION

Photonic crystals (PCs), whose dielectric properties change periodically at a period allowing for Bragg diffraction of light, attract interest as new optical materials with unique properties [1–4]. The localization of electromagnetic waves at structural defects is an important property of PCs [5–7]. In this case, additional allowed levels corresponding to localized defect modes appear in the bandgap of a photonic crystal. The positions and transmission coefficients of the defect modes can be effectively controlled by varying the geometrical and structural parameters of PCs. PCs with defect modes were used to create new types of photonic crystalline waveguides [8], high-Q nanocavities [9, 10], and low-threshold lasers [11, 12] and to propose new methods for increasing the efficiency of nonlinear optical processes [13–16]. If two embedded defect layers in a one-dimensional PC are located at a distance significantly larger than the size of an electromagnetic field localization region near a defect layer, the defect mode frequency is doubly degenerate. When the defect layers move toward each other, the resonance character of the mutual effect of the defect modes splits the frequency, a pair of frequencies shifted with respect to each other appears instead of this frequency, and one or two peaks are detected in the bandgap of the transmission spectrum of the PC. In other words, the frequency splitting results from the interaction of two localized optical modes in coupled cavities [17–20]. Note also that the splitting of coupled oscillators is identical to the vacuum Rabi splitting of the mode of an optical cavity filled with two-level atoms [21–23]. When the cavity (defect layer) of a one-dimensional PC is filled with a resonance gas, two absorption peaks are detected (in contrast to PC without the dispersion of a defect layer), when the resonance frequencies of atoms and the defect mode coincide. This specific feature in the absorption spectrum appears due to the splitting of the frequencies of the PC defect mode and an electronic transition in atoms, which were considered as two coupled oscillators. The splitting of the mode of an optical cavity filled with a resonance gas can be interpreted differently. A defect layer without atoms corresponds to a defect mode of a certain frequency, which is the eigenmode of the cavity. When the defect layer is filled with a resonance gas, the Fabri–Perot resonance condition changes because of the dispersion of the refractive index, and two eigenmodes of the cavity are the solution to the corresponding equation [22].

Composite media with metal nanoparticles are of great interest for creating nanostructured metal–insulator PCs and new methods of controlling light based on them [24, 25]. The resonance of an effective permittivity is predicted in a nanocomposite consisting of metallic nanoparticles suspended in a transparent matrix provided that the optical properties of the initial materials have no resonance features [26, 27]. The resonance position lies in the visible region and depends on the permittivities of the initial compo-

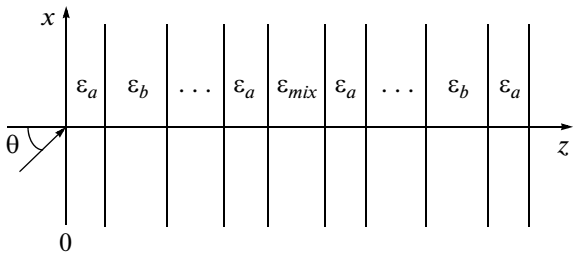

Fig. 1. Schematic representation of a one-dimensional PC structure with a lattice defect.

nents and the nanoparticle concentration and shape. The purpose of this work is to study the spectral properties of a one-dimensional PC with a resonance absorbing defect layer of a nanocomposite consisting of spherical silver nanoparticles randomly distributed in a dielectric matrix. We analyze the defect-mode splitting and the electromagnetic-field localization induced by a change in the volume fraction of nanoparticles in the defect layer. We also study the modification of the absorption spectrum during the variation of the angle of incidence and the structural parameters of the PC and defect layer.

2. MODEL AND THE DETERMINATION OF TRANSMISSION, REFLECTION, AND ABSORPTION

We analyze a PC structure consisting of a finite layered medium made of alternating layers of two materials with a structural lattice defect (Fig. 1).

As a defect layer, we chose a nanocomposite layer of thickness W_d consisting of metallic nanoballs dispersed in a transparent matrix. The defect layer is embedded between two identical superlattices with unit cells consisting of materials a and b with layer thicknesses W_a and W_b, respectively. This structure is characterized by nanocomposite permittivity $\varepsilon_{mix}(\omega)$. Hereafter, we assume that the medium in which the layered structure is placed is vacuum. Permittivity ε_{mix} is determined by the Maxwell–Garnett formula, which is widely used to consider matrix media containing dispersed isolated inclusions with a low volume fraction [26–30],

$$\varepsilon_{mix} = \varepsilon_d\left[1 + \frac{f}{(1-f)/3 + \varepsilon_d/(\varepsilon_m - \varepsilon_d)}\right], \qquad (1)$$

where f is the filling factor, i.e., the fraction of nanoparticles in the matrix; $\varepsilon_m(\omega)$ and ε_d are the permittivities of the nanoparticle metal and the matrix, respectively; and ω is the radiation frequency. The nanoparticle size is much smaller than the wavelength and the field penetration depth in the material. We find the permittivity of the nanoparticle metal using the Drude approximation

$$\varepsilon_m(\omega) = \varepsilon_0 - \frac{\omega_p^2}{\omega(\omega + i\gamma)}, \qquad (2)$$

where ε_0 is the constant that takes into account the contributions of the interband transitions of coupled electrons, ω_p is the plasma frequency, and γ is the reciprocal of the electron relaxation time.

Function $\varepsilon_{mix}(\omega)$ is a complex function,

$$\varepsilon_{mix}(\omega) = \varepsilon'_{mix}(\omega) + i\varepsilon''_{mix}(\omega). \qquad (3)$$

We neglect small factor γ^2 and find the resonance frequency position, which depends on the properties of the initial materials and the dispersed phase concentration f,

$$\omega_0 = \omega_p\sqrt{\frac{1-f}{3\varepsilon_d + (1-f)(\varepsilon_0 - \varepsilon_d)}}. \qquad (4)$$

At point $\omega = \omega_0$, function $\varepsilon'_{mix}(\omega)$ vanishes and $\varepsilon''_{mix}(\omega)$ becomes maximal. Function $\varepsilon'_{mix}(\omega)$ also vanishes at point

$$\omega_1 = \omega_p\sqrt{\frac{1+2f}{\varepsilon_0 + 2\varepsilon_d + 2f(\varepsilon_0 - \varepsilon_d)}}. \qquad (5)$$

In the interval $[\omega_0, \omega_1]$, function $\varepsilon'_{mix}(\omega) < 0$; that is, the nanocomposite in this frequency range is similar to a metal.

We study the spectra of transmission, reflection, and absorption of p-polarized waves propagating in the xz plane of the PC with a nanodefect using the transfer-matrix method [31]. The permittivities of the layers are specified as

$$\varepsilon = \begin{cases} \varepsilon(0) = 1, & z < z_0, \\ \varepsilon(1) = \varepsilon_a, & z_0 < z < z_1, \\ \varepsilon(2) = \varepsilon_b, & z_1 < z < z_2, \\ \cdots \\ \varepsilon(l_1) = \varepsilon_{mix}, & z_{l_1-1} < z < z_{l_1}, \\ \cdots \\ \varepsilon(N) = \varepsilon_b, & z_{N_1-1} < z < z_N, \\ \varepsilon(s) = 1. \end{cases} \qquad (6)$$

The magnetic-field distribution in the structure layers is written as

$$H_y(n, t) = [A_n e^{i\alpha_n(z-z_n)} + B_n e^{-i\alpha_n(z-z_n)}]e^{-i\omega t}, \qquad (7)$$

where A_n and B_n are the amplitudes of the incident and reflected waves in the nth layer, respectively,

$$\alpha_n = (\omega/c)\sqrt{\varepsilon(n) - \sin^2\theta}, \quad (8)$$

c is the velocity of light, and θ is the angle of incidence.

The electric-field distribution in the structure layers is

$$E_x(n, t) = \frac{c\alpha_n}{\omega\varepsilon(n)} \times [A_n e^{i\alpha_n(z-z_n)} - B_n e^{-i\alpha_n(z-z_n)}]e^{i\omega t}. \quad (9)$$

From the condition of continuity of E_x and H_y at the interface $z = z_{n-1}$, we obtain a set of equations that can be represented as the matrix equation

$$\begin{pmatrix} A_{n-1} \\ B_{n-1} \end{pmatrix} = T_{n-1,n}\begin{pmatrix} A_n \\ B_n \end{pmatrix}, \quad (10)$$

where the transfer matrix is

$$T_{n-1,n} = \frac{1}{2}\begin{pmatrix} (1+h)e^{-i\alpha_n\gamma_n} & (1-h)e^{i\alpha_n\gamma_n} \\ (1-h)e^{-i\alpha_n\gamma_n} & (1+h)e^{i\alpha_n\gamma_n} \end{pmatrix}, \quad (11)$$

$h = \alpha_n\varepsilon(n-1)/\alpha_{n-1}\varepsilon(n-1)$ are the thicknesses of layers $\gamma_n = z - z_{n-1}$, and $n = 1, 2, ..., N$. Equation (10) relates wave amplitudes A_0 and B_0 of the incident and reflected waves to wave amplitude A_s coming from the PC provided that the wave reflection from the right side of the PC is absent ($B_s = 0$),

$$\begin{pmatrix} A_0 \\ B_0 \end{pmatrix} = \hat{M}\begin{pmatrix} A_s \\ 0 \end{pmatrix}, \quad (12)$$

where

$$\hat{M} = \hat{T}_{01}\hat{T}_{12}\ldots\hat{T}_{N-1,N}\hat{T}_{N,S}, \quad (13)$$

$S = N + 1$, and $\gamma_{N+1} = 0$. The transmission coefficient is determined by the expressions

$$T(\omega) = \left|\left(\frac{A_s}{A_0}\right)_{B_s=0}\right|^2, \quad (14)$$

$$T(\omega) = \frac{1}{|\hat{M}_{11}|^2}, \quad (15)$$

where $\hat{M}_{11}$ is the element of matrix $\hat{M}$. Similarly, the reflection coefficient is

$$R(\omega) = \frac{|\hat{M}_{11}|^2}{|\hat{M}_{21}|^2}. \quad (16)$$

The absorption coefficient is

$$A(\omega) = 1 - T(\omega) - R(\omega). \quad (17)$$

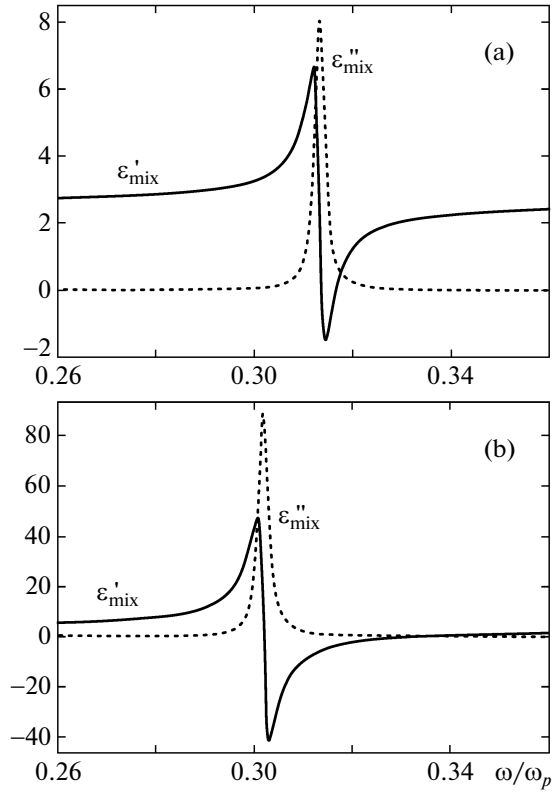

Fig. 2. Dependences of (dashed lines) imaginary ε''_{mix} and (solid lines) real ε'_{mix} parts of effective permittivity ε_{mix} on normalized frequency ω/ω_p. The filling factor is $f =$ (a) 0.01 and (b) 0.1.

3. CALCULATION RESULTS AND DISCUSSION

We now study the spectral properties of the PC with a defect nanocomposite layer by solving Eqs. (15)–(17) numerically and varying the medium parameters. For definiteness, we consider zirconium dioxide ZrO_2 with a permittivity $\varepsilon_a = 4.16$ and silicon dioxide SiO_2 with a permittivity $\varepsilon_b = 2.10$ as the materials of the alternating layers in the PC. The layer thicknesses are $W_a = 50$ nm and $W_b = 74$ nm, respectively.

The composite dielectric layer of thickness $W_d =$ 130 nm consists of silver nanoballs suspended in a transparent optical glass. For silver, we have $\varepsilon_0 = 5.00$, $\omega_p = 9$ eV, $\gamma = 0.02$ eV [32]; for glass, we have $\varepsilon_d = 2.56$. The frequency dependences of the real and imaginary parts of the permittivity calculated by Eq. (1) demonstrate that, as the volume concentration of nanoballs increases, frequency ω_0 corresponding to a resonance in the defect layer shifts toward low frequencies, the half-width of the resonance $\varepsilon''_{mix}(\omega)$ curve changes insignificantly, the $\varepsilon'_{mix}(\omega)$ curve changes significantly, and the frequency range where $\varepsilon'_{mix}(\omega) < 0$ increases.

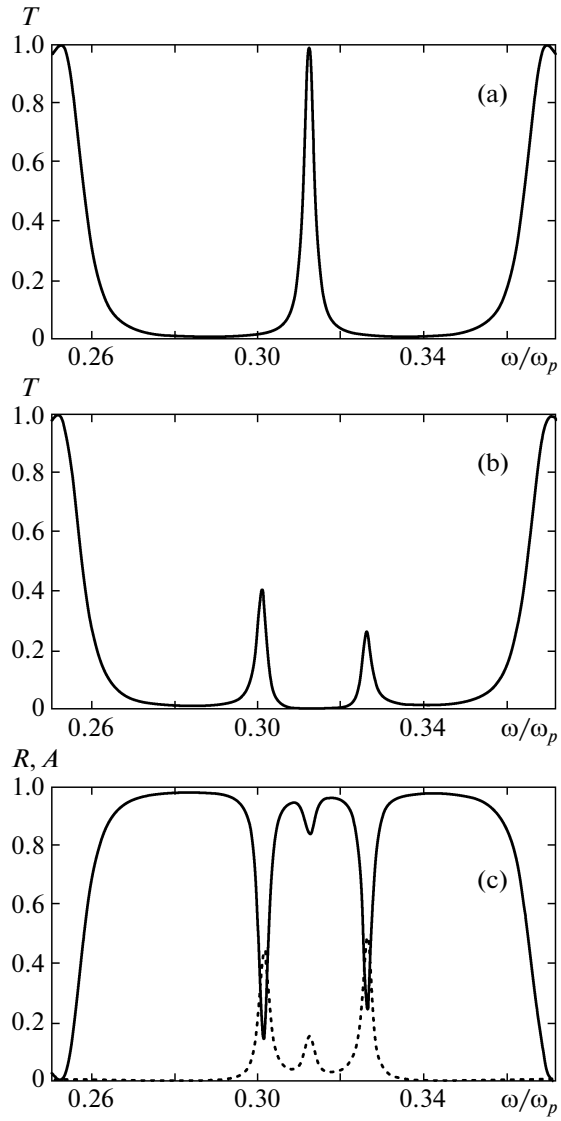

Fig. 3. Coefficients of (solid line) transmission T and reflection R and (dashed line) absorption A as functions of frequency for p-polarized waves. The filling factor is $f =$ (a) 0 and (b, c) 0.01, angle of incidence $\theta = 0°$.

As an example, Fig. 2 shows the $\varepsilon'_{mix}(\omega)$ and $\varepsilon''_{mix}(\omega)$ curves at two values of filling factor f.

Figure 3a shows the seed transmission spectrum of p-polarized waves for the normal incidence of light onto a PC consisting of $N = 19$ layers at $f = 0$ and other unchanged system parameters. It is seen that, at filling factor $f = 0$ (when dissipation is absent in the system), the PC is almost transparent for radiation with a frequency coinciding with defect-mode frequency ω_d, which is located near the center of the first bandgap. The bandgap is situated in the wavelength range 355–470 nm.

The frequency splitting effect in the transmission, reflection, and absorption spectra is illustrated in Figs. 3b and 3c, respectively, for the case where the filling factor is $f = 0.01$ and composite resonance frequency ω_0 coincides with defect-mode frequency ω_d. In contrast to the PC structure without the dispersion of the defect layer, there are two transmission peaks, which is caused by the dispersion and absorption in the defect. The splitting in the transmission spectrum is $\Delta\lambda \approx 34$ nm, which is two orders of magnitude larger than the mode splitting in a PC with similar parameters and a defect layer filled with a resonance gas [22, 23]. The frequency splitting is caused by the resonance situation that appears when the composite resonance frequency coincides with the defect-mode frequency.

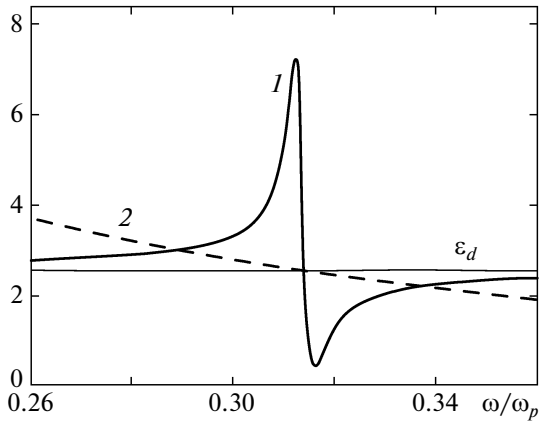

Fig. 4. Graphic solution to Eq. (18): frequency dependences of (*1*) n and (*2*) ω_R/ω. The filling factor is $f = 0.01$.

In other words, the frequency splitting effect is induced by a change in the Fabri–Perot resonance condition because of the dispersion of nanocomposite permittivity $\varepsilon_{mix}(\omega)$. The Fabri–Perot resonance condition has the form

$$n(\omega) = \frac{\omega_R}{\omega}, \qquad (18)$$

where

$$n(\omega) = \left[\frac{\sqrt{\varepsilon'^2_{mix} + \varepsilon''^2_{mix}} + \varepsilon'_{mix}}{2}\right]^{1/2},$$

$$\omega_R = \frac{\pi c m}{W_d}, \quad = 1, 2, \ldots$$

Figure 4 shows the graphic solution to Eq. (18).

Two cavity eigenmode frequencies are clearly visible in the transmission spectrum (Fig. 3b). The intermediate solution in the transmission spectrum does not appear because of high absorption. Without regard for losses ($\gamma = 0$), the transmission spectrum has the three peaks corresponding to the three solutions to Eq. (18): side peaks with $T = 1$ and an intermediate peak with $T = \infty$ because of the permittivity pole at the resonance frequency. The calculations at $\gamma \neq 0$ show

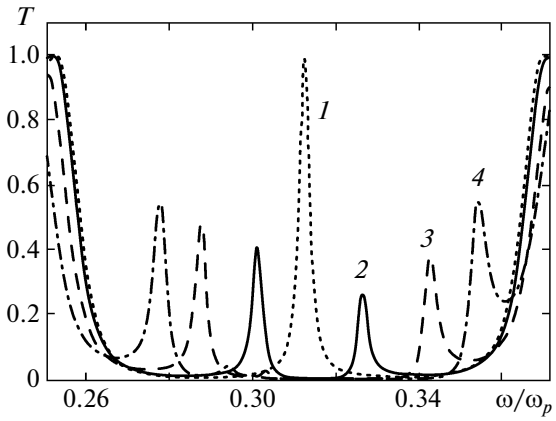

Fig. 5. Frequency dependences of the transmission coefficient at various filling factors at $\theta = 0$: (*1*) $f = 0$, (*2*) 0.01, (*3*) 0.05, and (*4*) 0.1.

that the peak positions are loss-independent; therefore, the change in the splitting induced by a variation in the filling factor is caused by a change in the $\varepsilon'_{mix}(\omega)$ dispersion curve (see Fig. 2).

Figure 5 shows the transmission spectrum at various filling factors. The splitting is seen to increase with the concentration of silver nanoballs in the defect layer: for example, when f increases from 0.01 to 0.1 (i.e., 10 times), the splitting increases threefold and is 101 nm.

For comparison, Fig. 6 shows the spatial electric-field distributions at the defect-mode frequency corresponding to the maximum transmission at $f = 0$ (see Fig. 3a) and at the high-frequency peak frequency at $f = 0.01$ (Fig. 5, solid line). It is seen that the field distribution inside the PC with a nanocomposite defect layer almost coincides with the field distribution in the defect region without dispersion. In both cases, the field is localized in a region comparable to the wavelength.

Figure 7 shows the dependence of the transmission spectrum on angle of incidence θ and nanocomposite defect layer thickness W_d. When θ or W_d changes, a mismatch between the nanocomposite resonance frequency and the defect-mode frequency $\Delta\omega = \omega_d - \omega_0$ appears. It is seen that the bandgap boundaries remain almost unchanged as the defect layer thickness decreases from 130 to 120 nm and that an increase in the angle of incidence from 0° to 30° according to the Bragg condition leads to their noticeable high-frequency shift. The frequencies of the two defect modes in the bandgap of the PC structure shift toward high frequencies with the same modification of the transmission peak shapes when the defect layer thickness decreases or the angle of light incidence increases. This behavior of the frequencies can be understood if we represent the defect mode of the PC structure in the form of a standing wave that appears as a result of

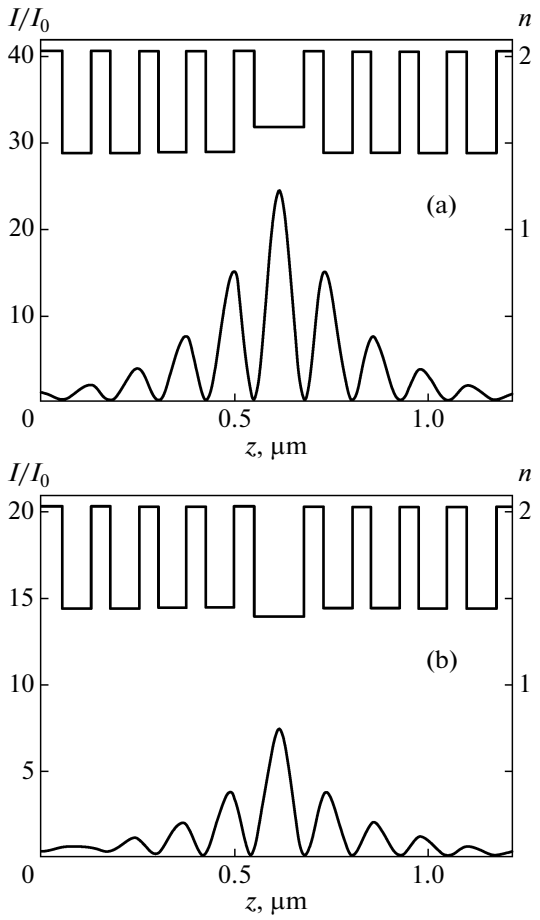

Fig. 6. Distributions of the refractive index and the field normalized by input intensity I_0 at $f =$ (a) 0 and (b) 0.01.

reflection from the walls of the cavity formed by a nanodefect of thickness W_d. If we also neglect the frequency dependence of the refractive index in the region of the transmission peaks, we can write the resonance condition in the form

$$\lambda = 2W_d\sqrt{n^2 - \sin^2\theta}.$$

Therefore, the mode frequencies shift toward high frequencies when thickness W_d decreases or angle of incidence θ increases, which is observed during numerical simulation.

A variable angle of incidence is a convenient parameter to qualitatively change the transmission spectrum of the PC structure. When angle of incidence θ increases, the low-frequency edge of the bandgap shifts toward defect layer resonance frequency ω_0. At $\theta = 55°$, the low-frequency peak in the bandgap of the transmission spectrum almost disappears and the high-frequency peak corresponding to the defect mode is retained. It is important that resonance frequency ω_0 at this angle of incidence is near the low-frequency boundary of the bandgap. Mixing

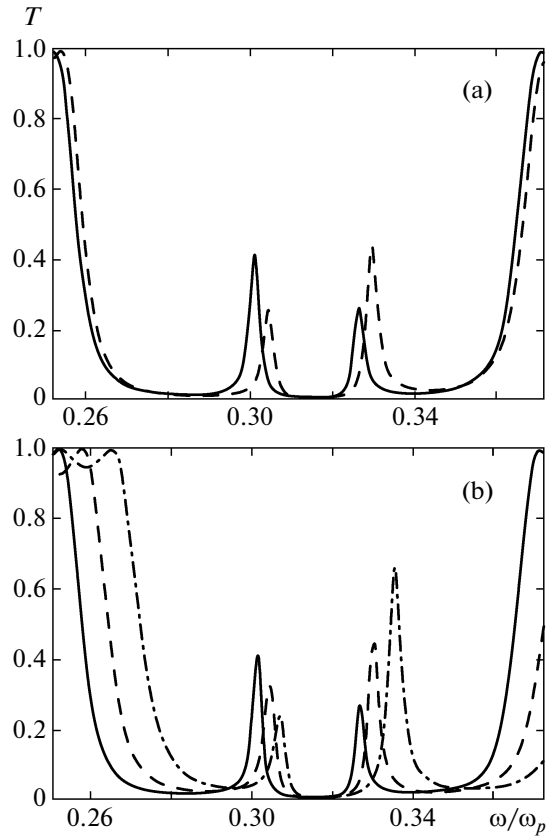

Fig. 7. Transmission spectra at various (a) defect layer thicknesses and (b) angles of incidence: (a) W_d = (solid line) 130 and (dashed line) 120 nm; (b) θ = (solid line) 0°, (dashed line) 20°, and (dot-and-dash line) 30°.

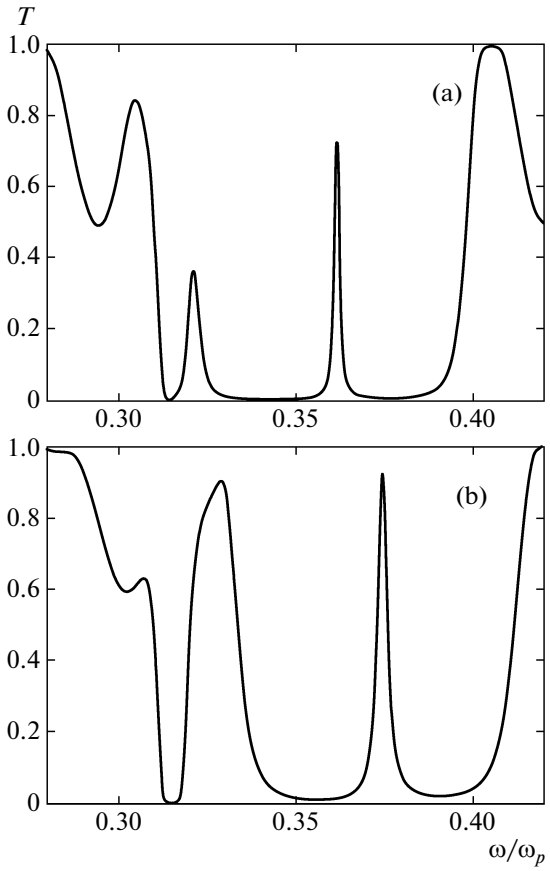

Fig. 8. Transmission spectra at various angles of incidence: (a) θ = 55° and (b) 65°. The filling factor is $f = 0.01$, the number of layers is $N = 35$, and the other parameters are identical to those for Fig. 7.

of the resonance mode with photon modes results in the bandgap splitting effect; that is, an additional 5-nm-wide transmission band appears in the bandgap (Fig. 8a). At θ = 65°, frequency ω_0 coincides with the frequency of the first side maximum of the continuous transmission spectrum, and the appearing resonance situation results in the appearance of an additional bandgap, whose width is approximately 10 nm, in the transmission spectrum (Fig. 8b). Note that these widths are four orders of magnitude larger than the transmission band width in the bandgap and the additional bandgap width in the transmission spectrum of a layered medium in which a resonance gas is one of the alternating layers [33].

4. CONCLUSIONS

We studied the spectral properties of a one-dimensional PC with a structural resonance absorbing layer of a nanocomposite consisting of silver nanoballs suspended in a transparent optical glass and revealed a number of important features in the transmission spectrum of the PC, which are mainly related to a resonance character of the effective permittivity of the nanocomposite and its substantial dependence on filling factor *f*. These results were obtained using the transfer-matrix method.

The splitting of the defect mode was shown to be very sensitive to nanoparticle concentration *f* and can reach 100 nm. The light field corresponding to the defect modes is localized near a defect in a region comparable to the wavelength. The transmission spectrum of the PC was shown to be controlled by changing the angle of incidence. At a given value of filling factor *f*, we found angles of incidence at which the transmission spectrum of the PC changes qualitatively: additional transmission bands and bandgaps appear. It is important that a PC with a defect nanocomposite layer filled with silver nanoballs makes it possible to work in the visible frequency region.

To calculate these features in the transmission spectrum of a PC, one can use the resonances of a defect layer filled with other metallic nanoballs with other PS structure sizes.

ACKNOWLEDGMENTS

This work was supported by projects nos. NSh-7810.2010.3, RNP.2.1.1.3455, 27.1 and 3.9.1 of the Russian Academy of Sciences, 5 and 144 of the Siberian Branch of the Russian Academy of Sciences, and State contract no. 02.740.11.0220 according to the program Research and Scientific-Pedagogical Brainpower of Innovated Russia.

REFERENCES

1. J. D. Joannopoulos, R. D. Meade, and J. N. Winn, *Photonic Crystals* (Princeton University Press, Princeton, New Jersey, 1995), p. 137.
2. K. Sakoda, *Optical Properties of Photonic Crystals* (Springer, Berlin, 2004).
3. K. Busch, S. Lölkes, R. B. Wehrspohn, and H. Föll, *Photonic Crystals: Advances in Design, Fabrication and Characterization* (Wiley, Weinheim, 2004).
4. V. F. Shabanov, S. Ya. Vetrov, and A. V. Shabanov, *Optics of Real Photonic Crystals: Liquid Crystal Defects and Inhomogeneities* (Siberian Branch of the Russian Academy of Sciences, Novosibirsk, 2005) [in Russian].
5. S. John, Phys. Rev. Lett. **58**, 2486 (1987).
6. D. R. Smith, R. Dalichaouch, N. Kroll, S. Schultz, S. L. McCall, and P. M. Platzman, J. Opt. Soc. Am. B **10**, 314 (1993).
7. A. M. Zheltikov, S. A. Magnitskii, and A. V. Tarasishin, JETP **90** (6), 600 (2000).
8. A. M. Zheltikov, Phys.—Usp. **43** (11), 1125 (2000).
9. P. Han and H. Wong, Opt. Lett. **29**, 192 (2004).
10. J. Vučković, M. Lončar, H. Mabuchi, and A. Scherer, Phys. Rev. E: Stat., Nonlinear, Soft Matter Phys. **65**, 016608 (2001).
11. Y. Akahane, T. Asano, B.-S. Song, and S. Noda, Nature **425**, 944 (2003).
12. O. Painter, R. K. Lee, A. Yariv, J. D. O'Brien, P. D. Dapkus, and I. Kim, Science (Washington) **284**, 1819 (1999).
13. B. Shi, Z. M. Jiang, X. F. Zhou, and X. Wang, J. Appl. Phys. **91**, 6769 (2002).
14. M. G. Martemyanov, T. V. Dolgova, and A. A. Fedyanin, JETP **98** (3), 463 (2004).
15. T. V. Dolgova, A. I. Maidikovskii, M. G. Martem'yanov, G. Marovsky, G. Mattei, D. Schuhmacher, V. A. Yakovlev, A. A. Fedyanin, and O. A. Aktsipetrov, JETP Lett. **73** (1), 6 (2001)
16. M. Soljačić and J. D. Joannopoulos, Nat. Mater. **3**, 211 (2004).
17. R. P. Stanlly, R. Houdre, V. Oesterle, M. Ilegems, and C. Weisbuch, Appl. Phys. Lett. **65**, 2093 (1994).
18. M. A. Kaliteevskii, Tech. Phys. **43** (5), 565 (1998).
19. S. Ya. Vetrov and A. V. Shabanov, JETP **93** (5), 977 (2001).
20. A. V. Shabanov, S. Ya. Vetrov, and A. Yu. Karneev, JETP Lett. **80** (3), 181 (2004).
21. Y. Zhu, D. J. Gauthier, S. E. Morin et al., Phys. Rev. Lett. **64**, 2499 (1990).
22. G. Khitrova, H. M. Gibbs, F. Jahnke, M. Kira, and S. W. Koch, Rev. Mod. Phys. **71**, 1591 (1999).
23. V. G. Arkhipkin, S. Ya. Vetrov, A. A. Zabolotskii, S. A. Myslivets, I. V. Timofeev, and A. V. Shabanov, in *Photonic Crystals and Nanocomposites: Structure Formation, Optical and Dielectric Properties*, Ed. by V. F. Shabanov, V. Ya. Zyryanov (Siberian Branch of the Russian Academy of Sciences, Novosibirsk, 2009), p. 72.
24. S. G. Tikhodeev and N. A. Gippius, Phys.—Usp. **52** (9), 945 (2009).
25. P. N. Dyachenko and Yu. V. Miklyaev, Opt. Mem. Neural Networks (Inf. Opt.) **16**, 198 (2007).
26. A. N. Oraevskii and I. E. Protsenko, JETP Lett. **72** (9), 445 (2000).
27. A. N. Oraevskii and I. E. Protsenko, Kvantovaya Elektron. (Moscow) **31**, 252 (2001).
28. J. C. Maxwell-Garnett, Philos. Trans. R. Soc. London **203**, 385 (1904).
29. A. V. Turik, G. S. Radchenko, A. I. Chernobabov, and S. A. Turik, JETP Lett. **79** (9), 407 (2004).
30. L. A. Golovan, V. Yu. Timoshenko, and P. K. Kashkarov, Phys.—Usp. **50** (6), 595 (2007).
31. P. Yeh, J. Opt. Soc. Am. **69**, 742 (1979).
32. P. B. Johnson and R. W. Christy, Phys. Rev. B: Solid State **6**, 4370 (1972).
33. A. M. Zheltikov, A. N. Naumov, P. Barker, and R. B. Miles, Opt. Spectrosc. **89** (2), 282 (2000).

Translated by K. Shakhlevich